ELSEVIER

Catalysis Today 37 (1997) 331–349

CATALYSIS TODAY

Catalyst deactivation by coke deposition: Approaches based on interactions of coke laydown with pore structure

R. Mann

Department of Chemical Engineering, UMIST, P.O. Box 88, Manchester M60 1QD, UK

Abstract

Catalyst deactivation by foulant deposition arises from interactions of the accumulating deposit with the geometry and void structure of particle porosity. Simple approaches involving a wedge-layering deposition in a parallel bundle of pores allow activity loss by surface coverage and pore plugging. More complex models use coking rates related to local concentration in bundles of randomly corrugated pores or in interconnected arrays of pore segments forming stochastic pore networks. Examples and illustrations are presented for cumene cracking on a supported zeolite catalyst. The optimal design of support pore structure to resist deactivation by coking is briefly discussed.

Keywords: Catalyst deactivation; Coke deposition; Pore structure; Fouling; Pore networks

1. Introduction

The chemistry and kinetics of catalysed hydrocarbon reactions are usually complex. Likewise, the geometry of the porosity of typical industrial catalyst particles seems intractably complicated. Their combination in conventional types of solid–fluid catalytic reactor usually provides only an overall measure of the outcome of the interactions of these complexities. As a result, many interpretations of deactivation behaviour where a relatively large amount of coke deposition takes place, have ignored pore structural issues and relied instead on empirical representations. Such empiricisms are in turn useless in providing information on the detailed interior processes which govern the overall result. Consequently, empirical approaches, such as those based on coke content [1], concentration [2] and the time-on-stream theory [3], provide no detailed understanding of the fundamentals of deactivation and thereby either prevent or at least discourage innovations in catalyst design which would deliver improved catalytic performance. In particular, such empirical approaches give no indication of how the active catalyst, the support and any associated promoters should be configured into a quantified architectural assembly designed to promote high reactivity, good selectivity, resistance to the deactivating consequences of coke deposits and sustained productivity in the face of activity loss. Experimental evidence has long been available to confirm that volumes of deactivating deposits can be sufficient to interfere significantly with the pore structure [4,5].

2. Distinguishing fouling, poisoning and sintering

In the approach to be adopted here, the above three mechanisms which can contribute to catalyst deacti-

PII S0920-5861(97)00023-0

vation need to be carefully classified and discriminated. This is because in many early studies, the analysis of catalyst activity loss by the adsorption of poisons onto a pore surface [6] was also applied to deactivation by foulant accumulation, so that the significant difference between them was lost and some confusion in terminology occurred.

Deactivation by poisoning refers to the adsorption of components onto active sites, so that they are poisoned and thereby inactive for the desired reaction(s). Implicit in this mechanism is that the small amount of adsorbed poison, whilst it may be sufficient to give a dramatic loss in reactivity, only accumulates onto the surface to form a very thin layer, most likely an incomplete monolayer, which then adds negligibly to the solid volume of the catalyst. Conversely, the accumulated surface poison does not interfere measurably with the catalyst/support pore volume.

In contrast, deactivation by fouling involves the accretion of significant amounts of foulant deposits onto the catalyst surface. These deposits can occupy a significant proportion of the pore volume and thereby can begin to distort the pore structure. Pore geometries can be significantly altered. The possibility of interference with access by diffusion and even the plugging of pores now arises. Thus whilst the accumulation of a surface deposit in poisoning does not necessarily demand a good understanding of the pore structure, fouling definitely requires some understanding of the layout of pore spaces if the consequences of the depositing foulant for reactivity are to be understood.

Finally, sintering here refers to distortions to the pore structure arising from thermal effects such that excesses in temperature or other consequent chemical interactions cause a softening, restructuring or even melting of the solid phases. The effect of this is to collapse the pore structure by some kind of solid coalescence processes, so that a loss of surface area occurs. As with fouling, a proper interpretation of this surface reduction requires a quantification of the pore structure.

The distinguishing of two of these three deactivation mechanisms can be seen from Fig. 1 in which a foulant deposit is accumulating in a simple model cylindrical pore of diameter D [7]. The pore surface beyond the penetration depth of the foulant, x, is fully active. However, the presence of the foulant covering

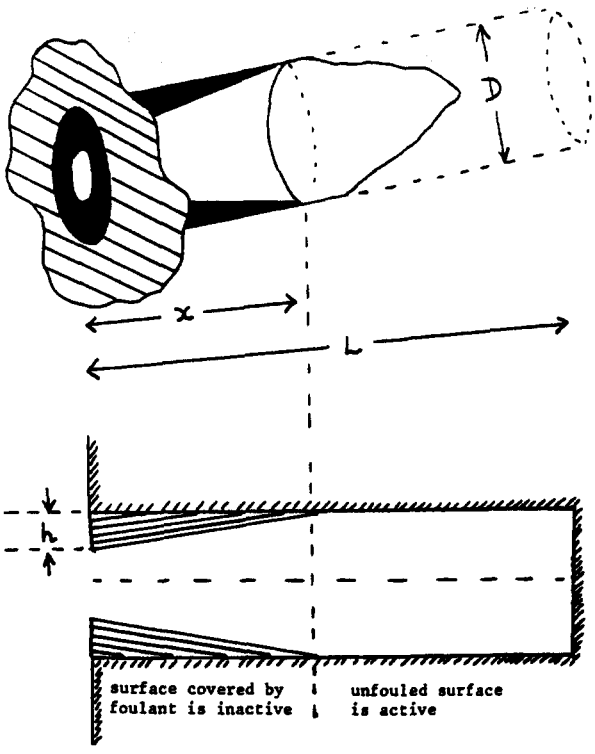

Fig. 1. Accumulation of a foulant deposit within a pore [7].

the pore surface renders it inactive, so that the coverage results in deactivation just as it would with poisoning [6].

However, as Fig. 1 clearly shows, the deposit occupies a significant part of the pore volume. The particular mode of accumulation in this case obeys a wedge-layering mechanism, which gives a pore mouth layer thickness h proportional to the penetration x. However, the deposit in the mouth of the pore will hinder access by diffusion and when h reaches $D/2$, the pore mouth will be plugged by the foulant deposit. Any "clean" interior surface not yet covered by the deposit will be, although potentially fully active, rendered inactive by the pore mouth plugging event.

The role of pore structure in influencing the deactivation process is then illustrated in Fig. 2, which shows the effect of variation in pore diameter [8]. For a simple wedge-layering foulant deposition like that in Fig. 1, activity is lost by surface coverage along the diagonal (which is equivalent to poisoning by surface

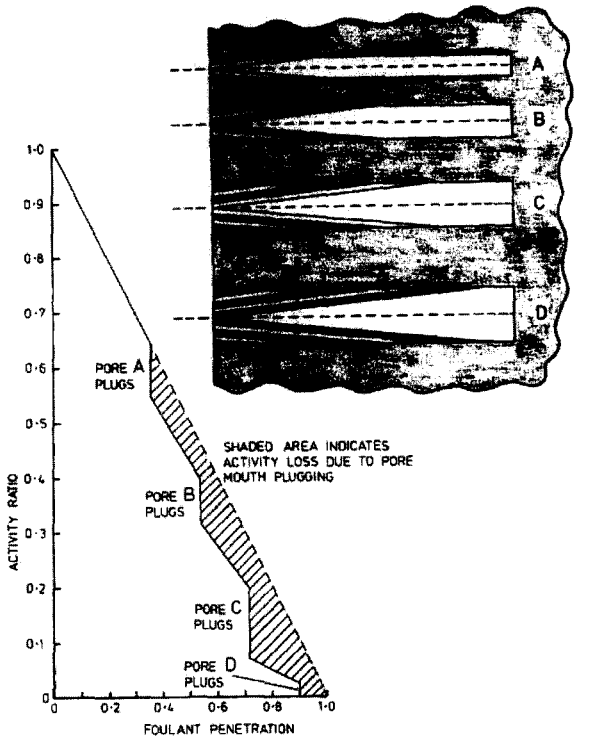

Fig. 2. Deactivation by fouling with pore size variation [8].

coverage without diffusional resistance Eq. (6)). However, the pore plugging, as it takes place in pores of increasing size, gives rise to the additional activity loss mechanism. In this way, the extent of deactivation is not simply linked to the degree of poison penetration. However, now coke content forms an additional measure of the deactivation process and plots of activity vs. coke content can be useful in delineating the deactivation mechanism [8]. Fig. 2 makes clear that interpretation of deactivation curves requires a quantitative description of the pore structure. This poses real difficulties as the pore structure of most catalysts is a complex randomised jumble of interconnected pore voids of irregular geometry and uncertain connective topology. It is therefore evident that, ultimately, a first principles basis for interpretation of catalyst deactivation by fouling relies as much upon a good quantification of the pore structure as it does upon our understanding of the basic diffusion and reaction processes that accompany catalysis in a porous particle.

3. Deactivation by wedge layering on a cracking catalyst

The first detailed application of the wedge-layering concept was for a commercial cracking catalyst (Super D manufactured by Crosfield Chemicals, Warrington, UK) using a parallel bundle of pores model [7]. This model envisages that the complex details of the catalyst particle porosity can be represented by an assembly of idealised cylindrical pores like that shown schematically in Fig. 2.

An interesting test of this fouling theory is to use it to interpret deactivation behaviour when the length dimension of the catalyst is changed. Fig. 3 shows experimental results for cumene cracking using pellets of length dimension 1.18 mm and 100 μm obtained on a fixed-bed activity test unit. In Fig. 3 the finely powdered particles have been made by grinding the larger pellets, so that the pore structures should be approximately identical in each case. The parallel bundle pore size distribution is then shown in Fig. 4 as a truncated log-normal distribution extending to 1 μm. The truncation at r=13 Å corresponds to the zeolite pore size. The zeolite pores contribute 98.5 $m^2\ g^{-1}$ and the parallel bundle pores of the support raise the overall specific surface to 133 $m^2\ g^{-1}$.

The effect of changing the pore length is then shown schematically in Fig. 5. An exploration of the two parameters of wedge layering, namely $\beta=x/h$ and the time for complete penetration which corresponds to complete deactivation, t_D, gives the theoretical results

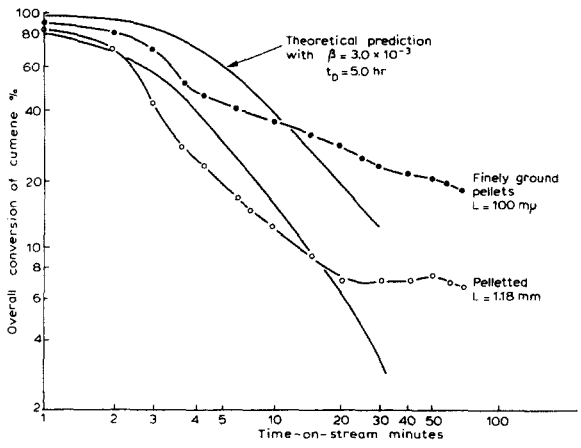

Fig. 3. Deactivation of an FCC catalyst by cumene cracking [7].

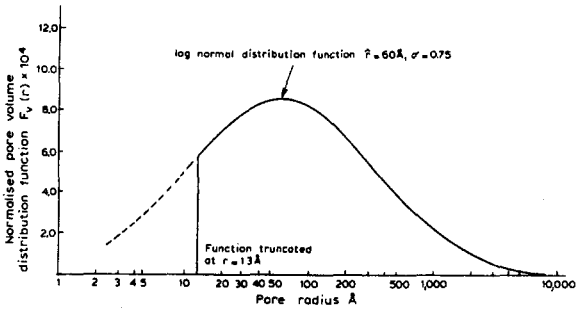

Fig. 4. Pore size distribution for Super D [7].

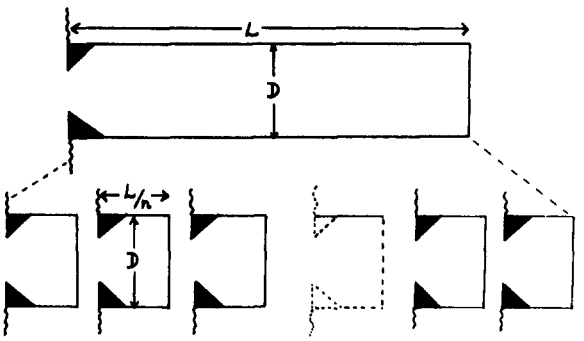

Fig. 5. Effect of reducing catalyst particle size by a factor N [7].

shown in Fig. 3. Although $\beta=10^{-3}$ indicates that the wedge layers are apparently relatively quite thin, because the pores are mainly of quite small diameter compared to the pore length, this value of β shows that deactivation is plugging dominated rather than poisoning dominated as depicted in Fig. 6. This figure shows that for poisoning to dominate the activity loss, β would need to be 10^{-5}, i.e., 100-times smaller.

This wedge-layering approach was able to independently predict the deactivation behaviour as the LHSV varied over a ten-fold range from 2.68 to 234.4 $cm^3\,g^{-1}\,h^{-1}$ and temperature varied from 350 to 500°C using a wedge-layering parameter β varying only from 1.5 to 5.2×10^{-3}. The slightly lower values of β at higher LHSV indicated that intermediate products of cumene cracking have a greater tendency to form coke. The small increase in β value for higher temperatures suggested that pore mouth plugging increases as the temperature is raised. Also it was clear that a superior replication of the shape of

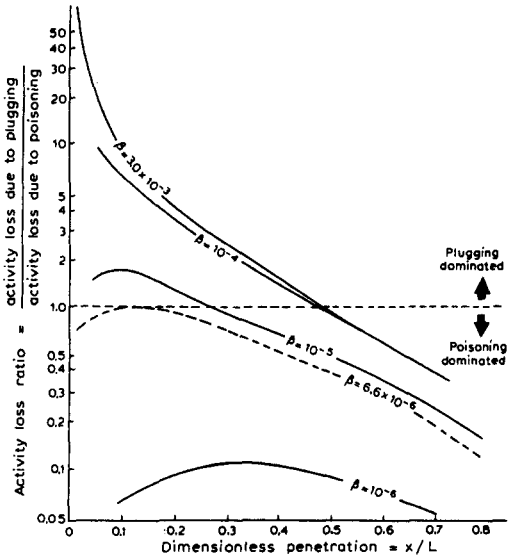

Fig. 6. Relative contributions of plugging and poisoning to activity loss [7].

the deactivation curve was obtained using a logarithmic rather than linear rate of coke penetration [7].

4. Impact of fouling on chemical selectivity

In the catalytic cracking of heavy oil fractions a critical factor in evaluating a particular catalyst is the selectivity of the reaction for the production of gasoline range components. These are intermediate products of the cracking process representing the most significant contribution to overall profitability. Any modelling of such a process involving a broad spectrum of reactants and products requires the "lumping" of groups of chemical species with similar kinetic behaviour. On this basis, many workers [9,10] have used very much simplified kinetic schemes, one of which is the lumped consecutive reaction scheme.

$$A \xrightarrow{k_{1s}} B \xrightarrow{k_{2s}} C$$

where k_{1s} and k_{2s} are catalytic surface reaction rate constants. Fig. 7 presents a graphical qualitative summary of the characteristic behaviour of the instantaneous pore mouth yield for a single sized cylindrical pore when fouling occurs in a hypothetical reactor using catalyst particles with single sized pores [11]. For the clean catalyst, when the penetration is zero, there is an intrinsic yield governed by the ratio of the surface reaction rate constants k_{1s} and k_{2s} in the absence of diffusional resistances. If the two consecutive reactions are both strongly influenced by diffusional resistances, there will be a significant yield taxation.

In the absence of diffusional resistances as penetration proceeds, there is no distinction between wedge layering and pore poisoning up to the point at which the pore mouth becomes sealed by the deposit. In this region the yield will be improving as the conversion achieved by the catalyst pores in the reactor declines. In the presence of strong pore diffusional resistance, Fig. 7 indicates the nature of the difference between poisoning dominated and pore plugging dominated wedge layering. At a given penetration of foulant, the additional resistance in the fouled section of the pore (nearest the mouth) may induce such an extra yield reduction that the decline in conversion may even be accompanied by a yield decline. In contrast, the poisoning dominated mechanism, involving as it does a thin layer of deposit, cannot give rise to a significant further dlffusional resistance and the behaviour is similar to that for poisoning and plugging in the non-diffusion influenced case. Ultimately in the plugging dominated case, the pores are likely to become sealed at partial penetration of foulant, so that the conversion decline to zero will happen suddenly and at an earlier stage than for the poisoning dominated case. This, however, does not show up on the reactor yield-

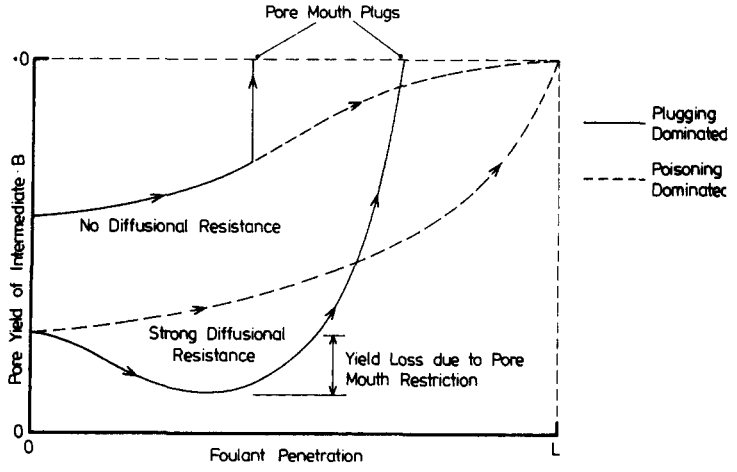

Fig. 7. Qualitative behaviour of pore mouth yield [11].

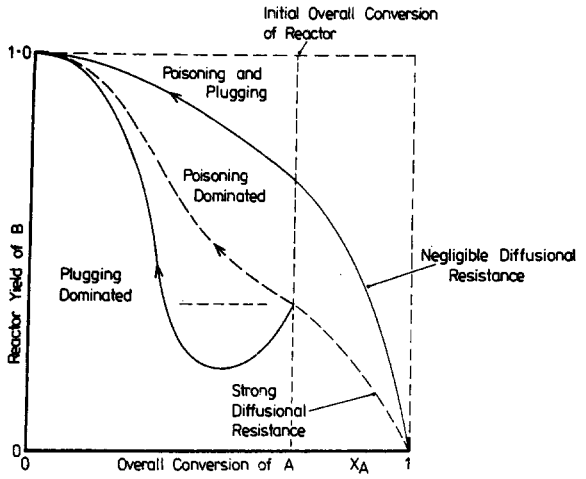

Fig. 8. Qualitative behaviour for a reactor with single pore size [11].

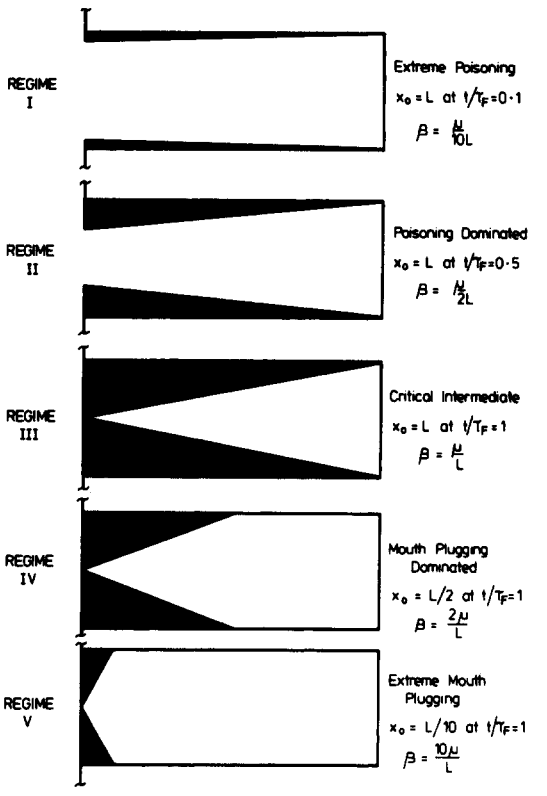

Fig. 9. Illustrative archetypes for deposition by wedge-layering [11].

overall conversion plot of Fig. 8, though it would be detectable on a conversion–time plot.

However, these simplified qualitative features for the uniform pore size case, become somewhat more complicated when a distribution of pore sizes is present. The penetration, plugging, activity and yield behaviour of a reactor will in this case be the net overall effect comprised of the summation over all the pore sizes present. When fouling of the catalyst takes place the active surface area is decreased by two factors. Firstly, small pores become rapidly sealed off initially when the foulant thickness becomes equal to the pore radius. Secondly, the active length of those pores not yet plugged is reduced by surface coverage.

In order to provide a thorough illustration of the theory, results will be presented for five classifications of fouling as shown in Fig. 9. These classifications are with reference to a dimensionless time scale of fouling

$$t/\tau_F = h/\mu \tag{1}$$

where μ is the mean pore size of the distribution under consideration and h depends upon time through the timewise penetration of foulant. This means that at a dimensionless fouling time of unity, the pore mouth thickness of foulant is just sufficient to plug those pores with a radius $r=\mu$. Fig. 9 has as extreme cases the classical pore mouth poisoning and pore plugging. In the case of extreme poisoning the thickness of the foulant approaches zero and a pore is completely deactivated when it has been completely penetrated. In contrast, for extreme pore mouth plugging, the mean pore size is sealed-off by the foulant at a small penetration. The intermediate regime case corresponds to the pore mouth plugging of the mean pore just at the condition where it has been fully penetrated. This condition corresponds to one of maximum accumulation of the foulant. The intermediate regime is flanked by poisoning dominant and pore mouth plugging dominant regimes. Each of the classifications of Fig. 9 corresponds to a particular value of the fouling parameter β, though in this case as the complexities for the consecutive reaction A → B → C unfold, it is easier to present results in terms of time on stream defined with respect to units of dimensionless fouling time given by t/τ_F.

The deactivation behaviour is qualitatively as expected, but the impact of fouling upon chemical

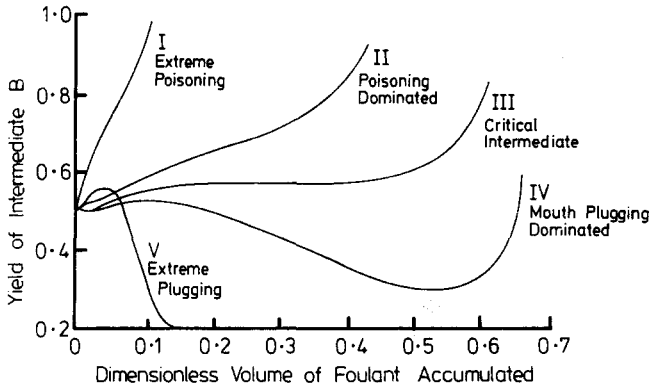

Fig. 10. Reactor yield of intermediate as a function of foulant accumulated [11].

Table 1
Reactor and catalyst properties for A → B → C

Pellet properties		Reactor properties	
Diffusivity	$D_A=0.144\times10^{-4}$ m^2 S^{-1}	Initial conversion	$X_A=0.90$
Diffusivity ratio	$\gamma=1.0$	Rate constant	$k_{1s}=0.46\times10^{-7}$ ms^{-1}
Bulk density	$\rho_b=0.79\times10^6$ gm^{-3}	Rate constant ratio	$N=0.4$
Pore volume	$\nu_g=0.2$ cm^3 g^{-1}	Initial A concentration	$C_{A0}=1.0$ kmol m^{-3}
Specific surface	$S_g=69.8$ m^2 g^{-1}	Initial B concentration	$C_{B0}=0.0$ kmol m^{-3}
Mean pore size	$\mu=70$ Å	Linear velocity	$u=0.4$ m s^{-1}
Variance of pore sizes	$\sigma=30$ Å	Bed density	$\rho=0.50\times10^6$ gm^{-3}
Minimum pore size	$r_{min}=10$ Å		
Maximum pore size	$r_{max}=4000$ Å		
Pore length	$L=0.75$ mm		

yield is more complex. This can be seen from Fig. 10 which shows the yield of B (the intermediate product) vs. time-on-stream for the five classes of fouling presented in Fig. 9. For the extreme poisoning case, as the conversion of A declines to zero, the yield of B rises almost linearly to unity. The initial value of yield for the reactor operating at 90% conversion of A is 0.45 which corresponds to the data shown in Table 1. As the fouling process moves towards a thicker mouth deposit accompanying the penetration, the ultimate yield when the activity is approaching zero shows a steady decline. This is due to the intensification of diffusional resistances caused by pore mouth thickening, hence reduced pore entry size, as well as the extra resistance arising from the deactivated section of the pore.

These diffusional effects produce some interesting variations in reactor yield in the regime of plugging dominated deactivation. Initially, small pores become blocked and since these have a low yield due to strong diffusional resistances impinging upon both reactions in the consecutive scheme, the overall yield begins to rise almost up to $t=\tau_F$. Then as penetration and thickening proceed in the larger pores around the mean radius, the additional diffusional resistances cause the yield to begin to decline, even though the associated decline in overall conversion is bound to improve the yield. Eventually, for the largest pores, their very low activity contribution (even when unfouled they contribute only fractionally to the overall conversion) is enough to offset the yield decline caused by diffusional resistances and the yield of the reactor then begins to rise. Even so, for the extreme pore mouth plugging case, the very smallest of conversions contributed by pores larger than $r=2\mu$ as far as $r_{max}=4000$ Å still have a very low fractional yield

of 0.2 and at $t=2\tau_F$, the yield is still declining as time proceeds. However, ultimately this yield curve would rise to produce a yield of 1.0 at zero conversion.

Nevertheless, Fig. 10 shows quite clearly that the simple physics and geometry of diffusion and foulant deposition produce somewhat complicated chemical effects. The simple two step chemical reaction A → B → C, when analysed with respect to a simple fouling model incorporating surface coverage and pore mouth plugging, can therefore show a complex rising–falling–rising pattern of overall yield behaviour with respect to time-on-stream. This rising–falling–rising pattern has been experimentally observed and closely replicated by this wedge-layering theory [11].

5. Extension to a supported zeolite catalyst

Mann and Thomson [12] extended the wedge-layering concept to allow discrimination between coke laydown in the silica\alumina support and coking in the zeolite crystallites. As before, their approach relied upon representing the support pore structure by a parallel bundle, but now three distinct zones can be present within a pore as shown in Fig. 11. The wedge-layer of foulant renders both the support and zeolite inactive. However, there is an intermediate portion of the pore where the zeolite has been deactivated, but cracking can still take place on the support surface. The most interior part of a pore then still remains fully active. In these circumstances, there is only diffusion within the wedge of foulant, but there is diffusion with only support reaction in the middle section.

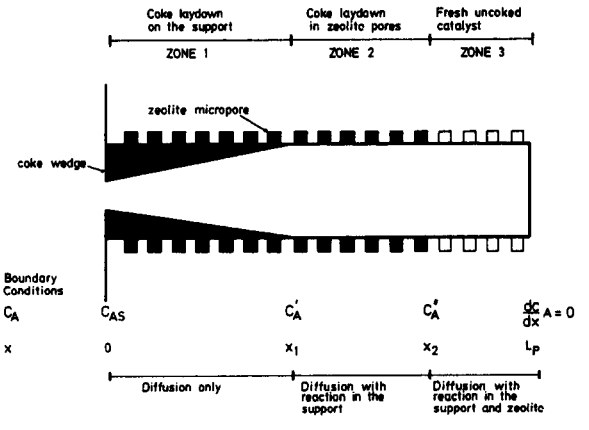

Fig. 11. Three idealised zones in zeolite catalyst support pore [12].

Different rates of deactivation (penetration) can be used for the support and the zeolite. Using this model, it is again possible to produce concentration and conversion profiles for the extremes of the theoretical deactivation process as well as intermediate conditions. As the deactivation process proceeds, the physical pore space structure of the catalyst is changed by coke being deposited in the support pores and zeolite micropores.

This change in pore structure can be observed by the use of low temperature capillary gas adsorption isotherms. Comparisons of isotherms for fresh and coked catalyst can then be a useful indicator as to the method of coke laydown and associated deactivation. Using equations and relationships developed by Broekhoff and de Boer [13], theoretical isotherms were produced for the parallel bundle (with the assumption that adsorption for any accessible zeolite occurred at a relative pressure close to zero) for each of the cases under study.

Fig. 12 shows some illustrative concentration profiles in a 500 Å radius pore for a high and a low value of β as a function of time. With the plugging mechanism, a rapid decrease in the size of the pore mouth occurs, causing an increase in the diffusional resistances and resulting in a steep linear region for the diffusional part of the profile. On the other hand, with a low value of β, there is negligible thinning of the pore mouth, resulting in a completely different evolution of the concentration profiles as deactivation proceeds [12].

Fig. 13 then shows some illustrative theoretical isotherms for deactivation mechanisms with different extents of pore plugging. Fig. 13a shows the isotherms for a mechanism in which no plugging occurs. The isotherms for the coked catalyst resemble the shape of the isotherm for the fresh catalyst but are displaced downwards towards the x-axis. This is to be expected, as with this mechanism of deactivation, the main site of coke laydown is in the zeolite micropores, not the support macropores. Further evidence that little coke laydown occurs in the support macropores is obtained from the fact that there is only a small change in the isotherms at 50 and 100 min. Because of the deactivation parameters chosen (complete zeolite deactivation in 50 min, support in 100 min) any difference between

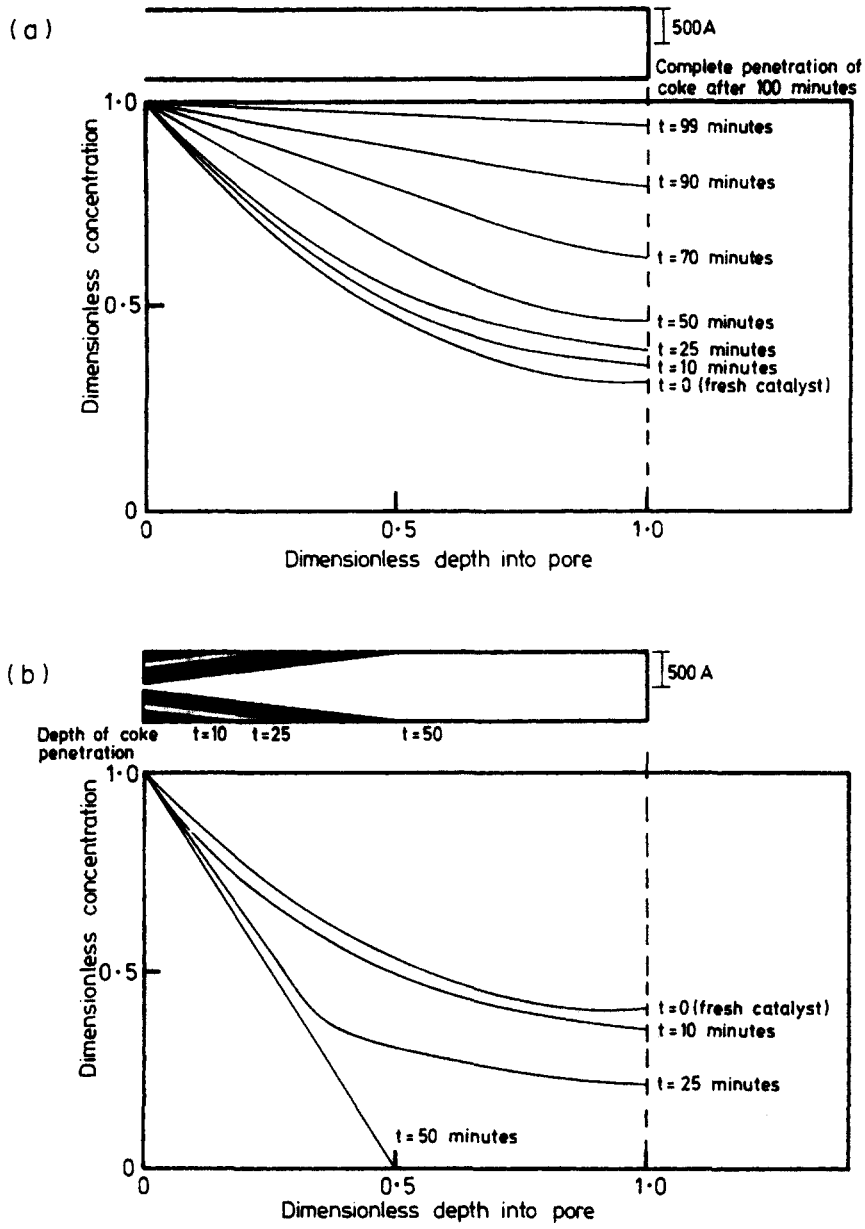

Fig. 12. Concentration profiles in a 500 Å support pore [14].

these isotherms has to be due to a change in the support structure, i.e., due to laydown of coke upon the support. Fig. 13b and c show the isotherms of a deactivation mechanism with an increasing amount of plugging. This increase in the amount of plugging manifests itself by producing isotherms that are compressed (as compared to the fresh isotherm) and have a flat adsorption branch. As the extent of plugging increases, so does the amount of compression and flattening.

Because of the difference in the conversion profiles and adsorption isotherms for the different values of β,

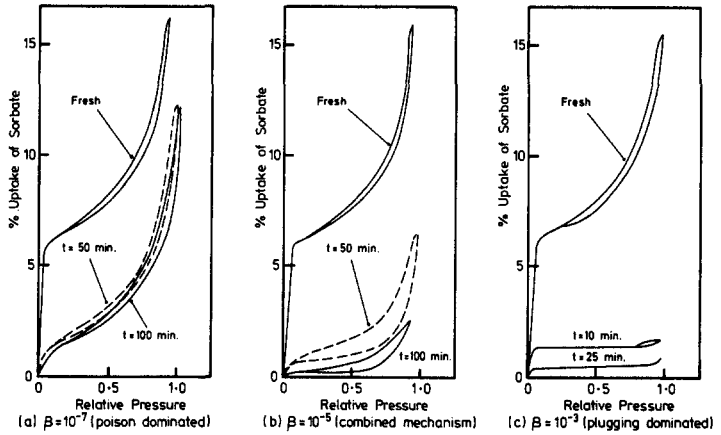

Fig. 13. Isotherms for fresh and coked catalyst pellets [14].

it ought to be possible to discriminate the method of deactivation based on observations of this kind. Experimental results for the cracking of cumene at 500°C [12] indicated a rapid loss of zeolite activity followed by a slower support deactivation which included the plugging of pores smaller than 150 Å in diameter.

6. Diffusion, reaction and coking in randomly corrugated pores

Two major deficiencies in the previous approaches are the use of bundles of uniform diameter pores and the invoking of a wedge type laydown mechanism which is uncoupled from the diffusion and reaction of coke precursors (whether these are reagents or products). Thomson [14] has advanced the modelling considerably by introducing randomly corrugated bundles of parallel pores and by linking coke laydown rates to local concentrations in the support pore assembly.

Fig. 14 shows schematically how an assembly of support pores appears if they are randomly corrugated. As before, the zeolite micro-pores are uniformly configured adjacent to the support pore surface. This arrangement of randomly large and small pores is much more realistic than the conventional parallel bundle, since it allows for constrictions between larger pores to arise naturally. When coke is laying down on the support, such adventitious constrictions can more easily become plugged and this form of pore blocking is expected to arise whenever significant amounts of coke accumulate on the support. The sealing off of interior portions of the catalyst, which would otherwise be active, could be a major factor in the character of any observed deactivation when pronounced amounts of coke accumulate.

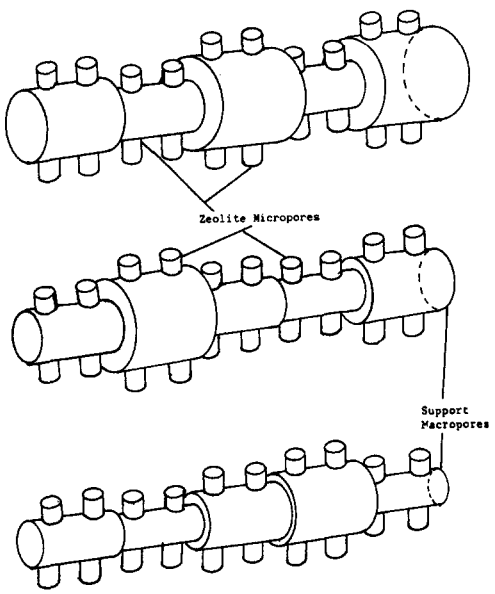

Fig. 14. Randomly corrugated support pores [14].

In abandoning the simplifications of wedge-layering, Thomson [14] and Sharratt [15] devised a local laydown mechanism based on the rate of coke deposition as a random deposition of individual coke units of diameter d. These units deposit sporadically on the support surface but may also deposit on one another, with an overall rate of deposition being governed by the localised concentrations of coke precursors. This leads to an apparently complex chaotic accumulation which nevertheless has a simple outcome in terms of the averaged coke layer thickness in a local pore segment (assumed locally uniform in concentration). This process is depicted in Fig. 15, where part of a pore segment of radius $D(0)$ has accumulated a coke layer of average thickness $h(t)$ after some time t. After sufficient further time, when the average coke layer thickness reaches $D(0)$, the pore segment becomes blocked.

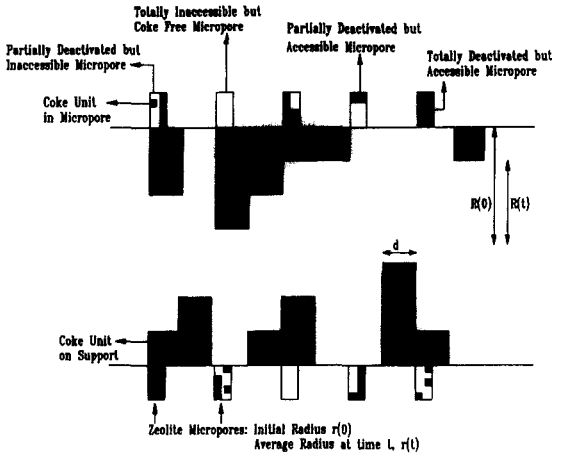

Fig. 15. Zeolite and support coking in randomly corrugated support pores [14].

This approach can incorporate the rate of reaction and rate of deactivation of the zeolite component. This is especially simple if the deactivation process in zeolite elements is made analogous to the balance of poisoning and fouling that is taking place on the adjacent support surface. This means that the zeolite deactivation is quantified by simple inference. However, it is useful to deploy this device to quantify zeolite behaviour without having to solve the full complexities of poisoning and fouling inside each zeolite crystallite. This inference by analogy has not been rigorously analysed so far, although the alternative of coupling detailed intra-zeolite processes with diffusion, reaction and coking in the support seems impossibly difficult at present.

The four possible "states" of zeolite deactivation are also indicated in Fig. 15. A totally inaccessible but coke-free micro-pore is created when a macro-pore coke-unit happens to deposit initially across a zeolite. A partially deactivated but inaccessible micro-pore

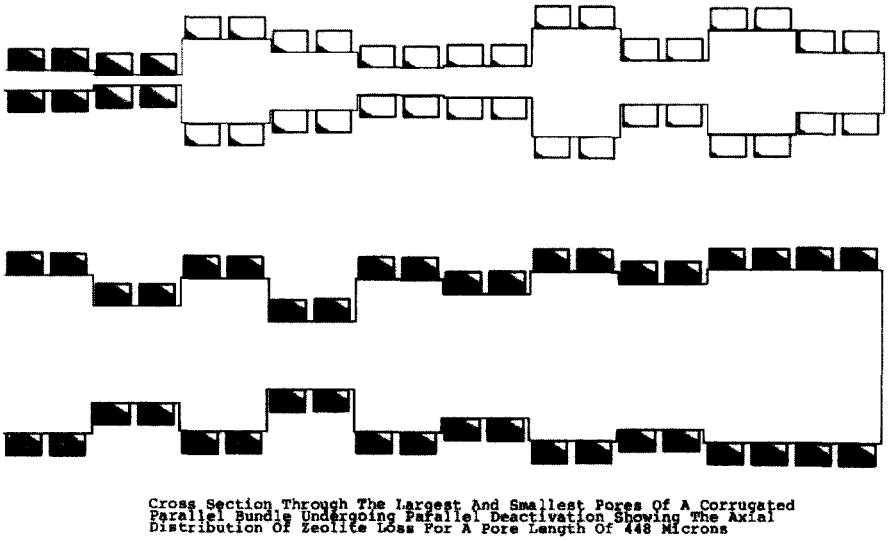

Fig. 16. Zeolite coke profiles in largest and smallest support pores [14].

arises when a support coke-unit happens to deposit some time later, when some reaction and coking have been able to take place within the zeolite. Finally, the two classes of micro-pore that can exist on uncoked surface of the support are then accessible and either partially or totally filled with coke. A fully coked micro-pore, whilst still accessible from the support pore space, would contribute nothing to reactivity.

If coke units of cubic size d are laid down randomly on the support surface, allowing laydown of one coke unit on top of another (as shown schematically in Fig. 15), the proportion of the surface covered to a depth of n units has a Poisson distribution

$$\theta_n = e^{-\lambda}\lambda^n/n! \quad (2)$$

and the mean depth is simply λ units [15].

This approach was applied to examine the deactivation of FCC cracking catalyst (Super D) for short reaction times in a fluidised bed micro-reactor. Illustrative intra-particle predictions are shown in Fig. 16 for the largest and smallest pores in a set of corrugated pores each made up from 10 segments, forming a typical particle of dimensions 448 μm. The randomly created largest pore exhibits no diffusional resistance. As a result, the zeolite is uniformly partially deactivated. In contrast, the smallest pore, which happens to possess two very small pore segments at its mouth, shows a distinct pore length change in zeolite coke content. There is a sudden change (reduction) after the second pore segment which severely restricts access to the remaining interior segments by virtue of the small cross-section restricting the diffusive flux through it. A slight further decline in zeolite coking can be seen along the remaining more interior pore segments. All the other pores in the bundle (198 out of the population of 200) have intermediate diffusional resistance and show intermediate zeolite coking.

Fluidised bed reactor simulations using the data shown in Table 2 replicated the reactor deactivation behaviour over a range of space velocities [14]. The predicted isotherms for O_2 corresponded closely with those measured experimentally as shown in Fig. 17.

Table 2
Data used in supported zeolite deactivation model for cumene cracking over Super D

Reaction and other constants	
Rate constant	6×10^{-8} m s^{-1}
Diffusion coefficient	1×10^{-6} m^2 s^{-1}
Feed concentration	14 kmol m^{-3}
Pellet mean size	2×10^{-3} m
Coking parameters	
Support coke size	20 Å
Zeolite coke size	3.7 Å
Activity ratio (zeolite/support)	0.3
Coking rate constant	3×10^{-1} m^2 s^{-1} kmol^{-1}

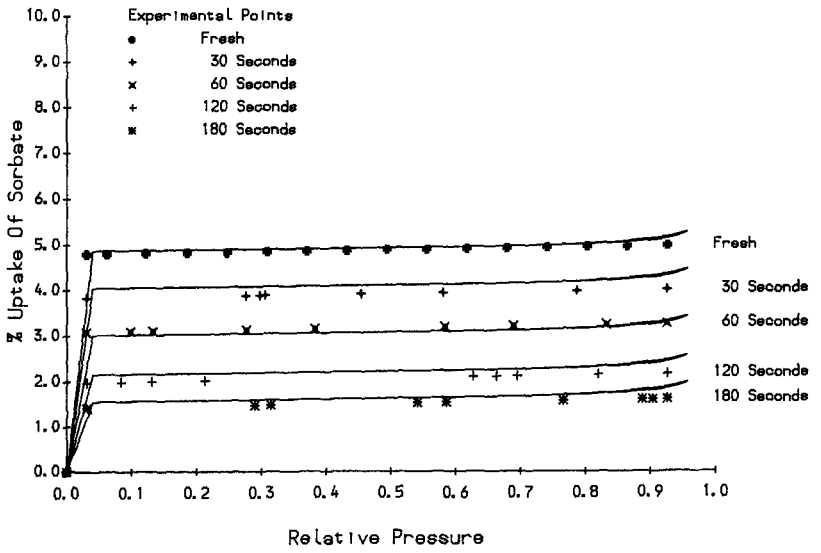

Fig. 17. Oxygen isotherms for cumene cracking on Super D [14].

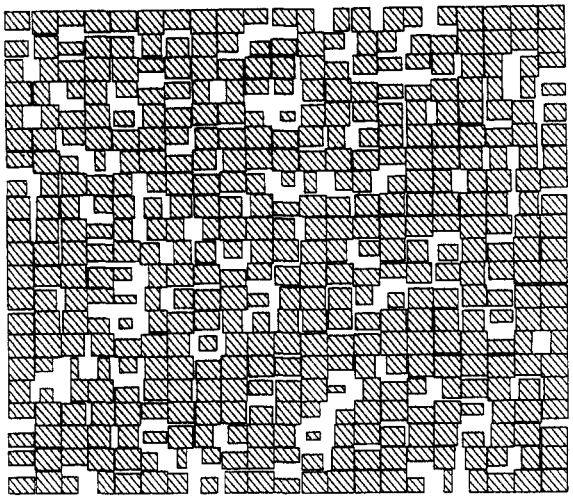

Fig. 18. Stochastic pore network for Super D [16].

At these short times on stream (<3 min), deactivation arises from coking of the zeolite, with negligible coke deposition on the support. The isotherms in Fig. 17 correspondingly show no detectable hysteresis loop. Moreover, at each time, the arm of the isotherm is almost horizontal, confirming almost no change in the support pore structure as a result of negligible coking.

7. Diffusion, reaction and coking in stochastic pore networks

Fig. 18 shows an image of a 2D stochastic pore network having a support pore size distribution matching the mercury penetration curve [16,17]. Such stochastic pore networks have sets of cylindrical pore segments interconnected together, but the size of any pore is independent of the neighbour pores. As with the corrugated pore model in Fig. 14, these networks have large pores randomly shielded amongst smaller ones, but in a network there is greater accessibility, so that the deactivating consequences of pore plugging are reduced. Such stochastic pore networks seek to make tractable the complexities of the chaotic pore spaces in a typical catalyst support.

This approach was successfully applied to observations of the deactivation of Super D cracking cumene at 500°C [16] in a plug flow reactor. This presents a greater complexity than a backmixed fluidised bed, and the microactivity tests ran for up to 2 h. Extensive deactivation took place as shown in Fig. 19. There is in this case axial deactivation along the fixed bed, measured by using 1,3 and 5 layers of catalyst.

Coking in each pore segment used the same approach already indicated in Fig. 15. For a single cylindrical pore, the diffusion/reaction equation for

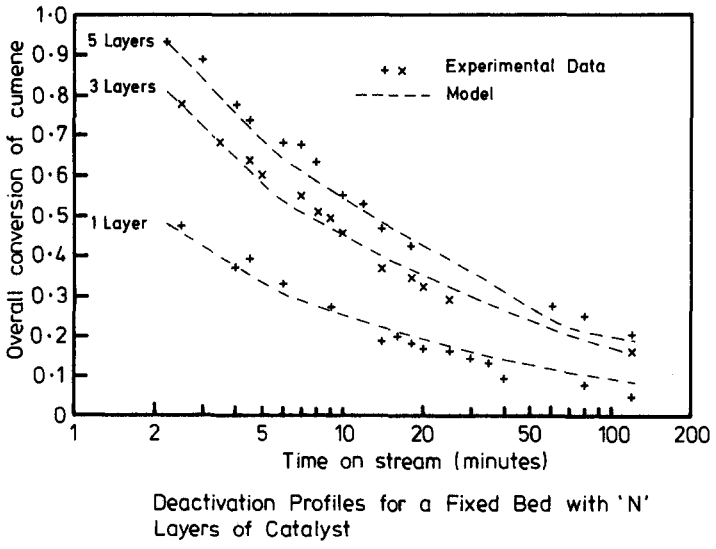

Fig. 19. Predicted and experimental deactivation profiles [16].

first order reaction is

$$D\frac{d^2C}{dx^2} - kC = 0, \quad k = 2\frac{k_s}{r}. \tag{3}$$

This may be solved, subject to the boundary conditions

$$x = 0, \quad C = C_1, \quad x = L, \quad C = C_2$$

to give the total flow entering the pore at x=0 as

$$N_i = \pi r_i^2 \sqrt{\frac{2k_{si}D}{r_i}} \left[\frac{C_1}{\tanh\phi_i} - \frac{C_2}{\sinh\phi_i}\right]. \tag{4}$$

Now consider a stochastic pore network assembled from a number of cylindrical pores in a square grid. Assuming that the rate of reaction at a node in the network is negligible, the net outflow from that node, summed over all connected pores, is zero. For an m connective node this can be expressed as follows:

$$\sum_{i=1}^{m} N_i = 0. \tag{5}$$

Substitution of Eq. (4) into Eq. (5) leads to an equation which is linear in the concentrations at the node in question and the m surrounding nodes. Such an equation can be written for each of the n^2 nodes in an $n \times n$ network. For nodes at the boundary one or more of the concentration terms will be equal to the external concentration. These equations are most conveniently expressed in a matrix form

$$\mathbf{A} \cdot \mathbf{c} = \mathbf{b}. \tag{6}$$

For the square network (m=4) the matrix **A** is sparse. A Gaussian elimination method was used, modified to perform only non-trivial operations. Iterative methods were found to converge slowly, if at all.

The solution of Eq. (6) is the set of node concentrations. From the node concentrations it is straightforward to calculate the total network reactivity. For each pore in the network, the change in coke depth with time was predicted by integration of the coking rates. At each time step, the node concentrations were recalculated using the current pore radii and activities. Fig. 20 shows the effect of support pore coking in the network of Fig. 18.

The adsorption/desorption process was again modelled using the equations developed by Broekhoff and de Boer [13]. In calculating the adsorption branch of the capillary adsorption isotherm it was assumed that the network position of the pores was of no importance and that sorbate condensation in any pore occurred at the pressure corresponding to the radius of that a pore. However, in calculating the desorption branch of the isotherm, evaporation of sorbate from pore could only occur if there was a path from that pore to the network surface. The desorption was carried out in a series of pressure reduction steps and a search algorithm employed at each of these steps to identify those pores linked to the surface of the network.

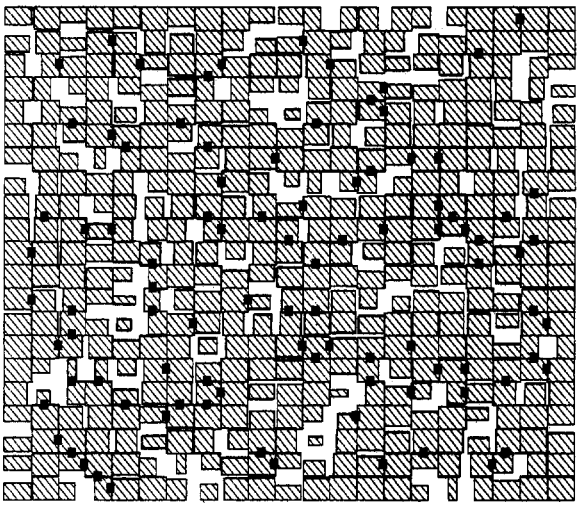

Fig. 20. Predicted coke laydown within catalyst particle [16].

The structural changes in the catalyst are then indicated by changes in the shape of the adsorption isotherm (Fig. 21). Experiment and theory show a high degree of correlation in the isotherms for both fresh and coked catalyst. The isotherms for the coked catalyst show a reduction in the range of pressures over which the hysteresis occurs in comparison with the fresh catalyst. The main cause of the hysteresis in the fresh catalyst is the so-called "bottle-necking" effect due to the high proportion of small pores (r<50 Å) in the pore size distribution. The reduction in pore radius that occurs after 2 h on stream leads to a loss of a large percentage of these small pores, resulting in a reduction in the size of the observed hysteresis.

A better indication of how coke accumulates has been visualised in Fig. 22, showing stages of layering within a network for increasing times on stream. For a sufficiently long time on stream, coke eventually fills

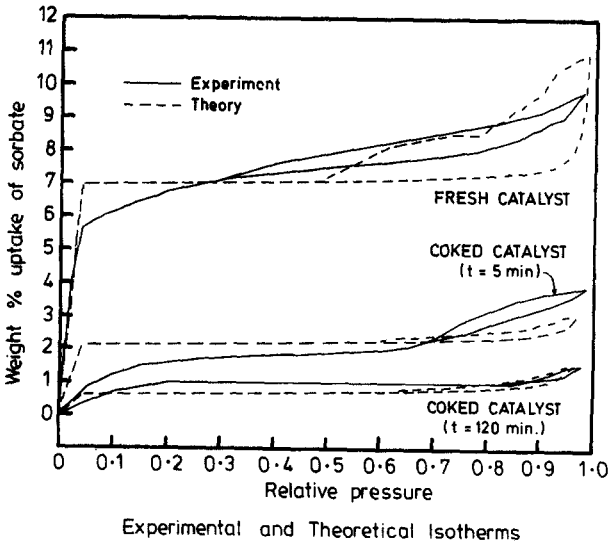

Fig. 21. Predicted and experimental oxygen isotherms [16].

up all the outermost pores. At this point, the catalyst particle is completely deactivated although the pore volume is not completely filled with coke. Random "pockets" of partially coked pores can be seen. These are formed when surrounded by smaller pores which have plugged earlier in the laydown process. Initially, comparing Fig. 22a and b, smaller pores do fill with even a thin layer of coke, but isolation by plugging has not yet occurred. The large square void in the top left corner of the network exemplifies this "isolation by plugging" process. In Fig. 22c this void is just still accessible by a single narrow unfilled pore, which then becomes sealed in Fig. 22d, leaving a prominent "square" unfilled void made up from four connected pores. Other voids with random shapes evolve as the network chokes up. In Fig. 22e, just six of the outermost pores remain active in the final stages of deactivation.

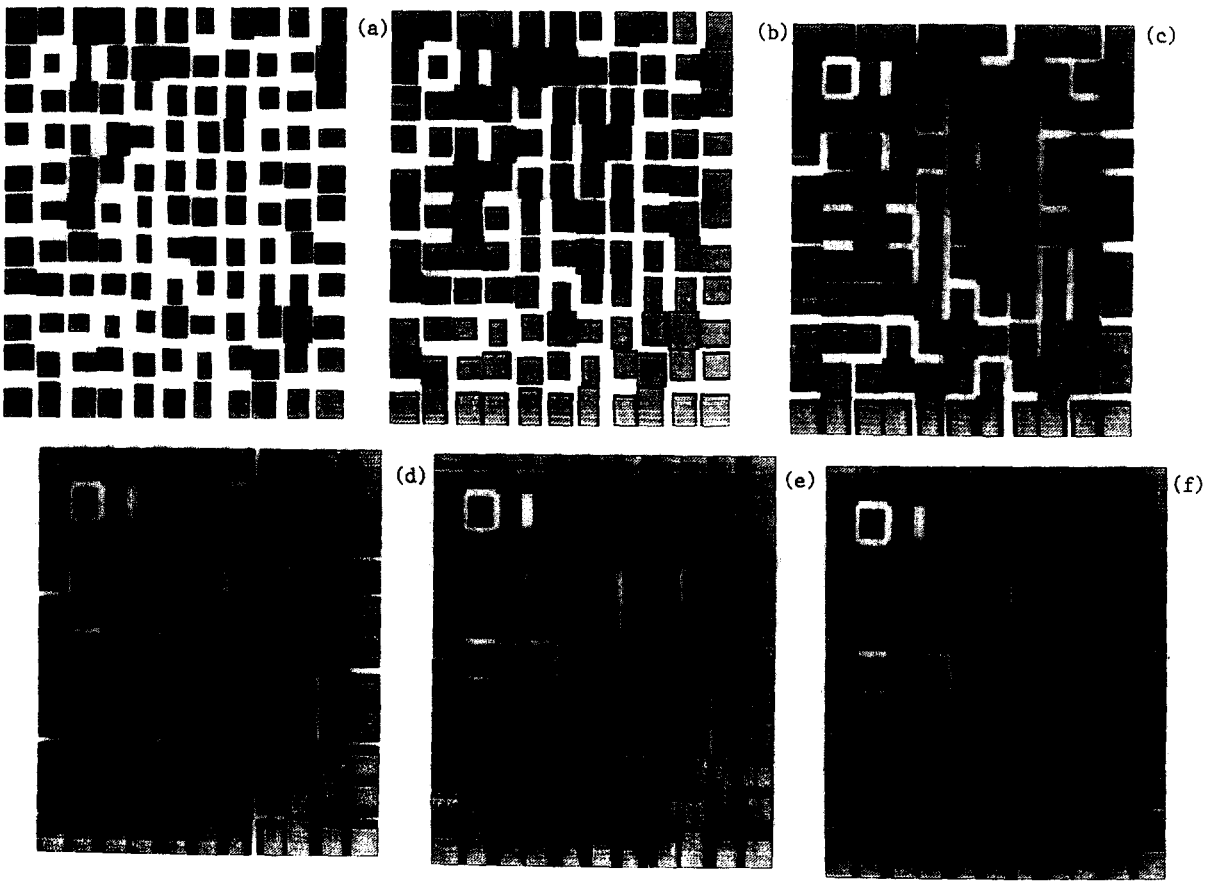

Fig. 22. Heavy coke accumulation in a 2D pore network [18].

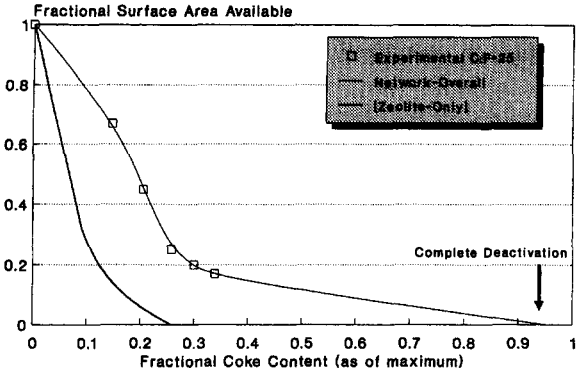

Fig. 23. Zeolite and support area loss as a function of coke content [18].

The results in Fig. 22 apply to some heavy coking results for a powdered Super D for which the calculations are comprehensively predictive. They can be presented alternatively as an accessible surface area vs. coke content as shown in Fig. 23. In this case, the zeolite component has rapidly lost its activity and become coked and the support after the maximum reaction time of 120 min has lost 83% of its surface.

The predicted behaviour shows that the support would, after a considerable further time, eventually fill with 95% coke content which corresponds to Fig. 22e. The support pore network is better able to accommodate large accumulations of coke than its counterpart randomly corrugated model (as in Fig. 14), although both structural models are capable of reproducing the experimental observations [18]. The stochastic network, because it provides for greater realism, almost certainly gives a better picture of this deactivation.

8. Extending to pore networks in 3D

Simple 2D networks provide insights into the deactivating effects of coking in a random mass of interconnected catalyst pores. Ultimately, however, full realism can only be achieved using networks in 3D. Fig. 24 shows a perspective view of a simple 3D stochastic pore network of size 15×15×15. This has a pore connectivity of 10 and is cubic with equal length pores. It can be further randomised by random displacements to the node positions. This produces variable length pores and a consequent cubic irregular

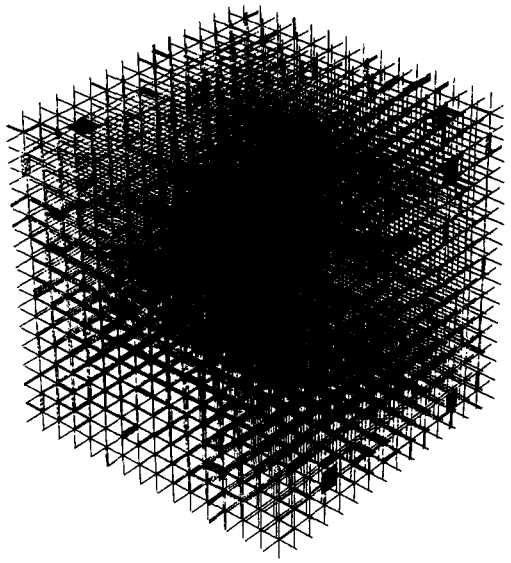

Fig. 24. A simple 15×15×15 cubic stochastic pore network.

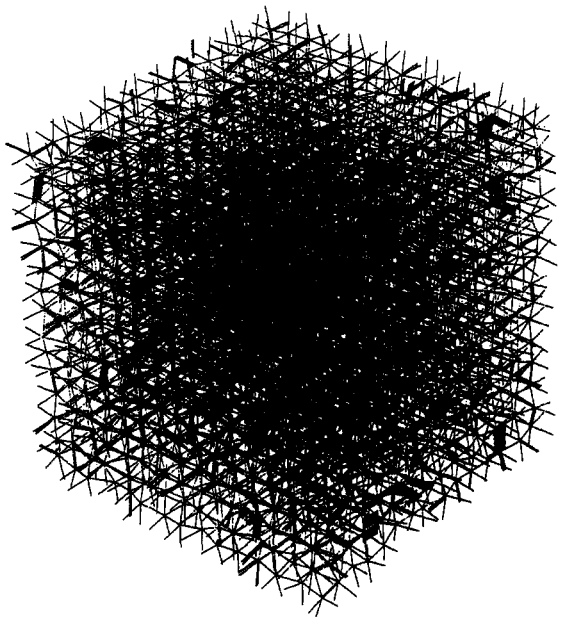

Fig. 25. Randomised irregular version of network in Fig. 24.

network is depicted in Fig. 25 for a maximum node displacement [19]. This further randomised network has the important property of retaining the simpler connective topology of the regular cubic network, so that the algorithms for mercury porosimetry and low

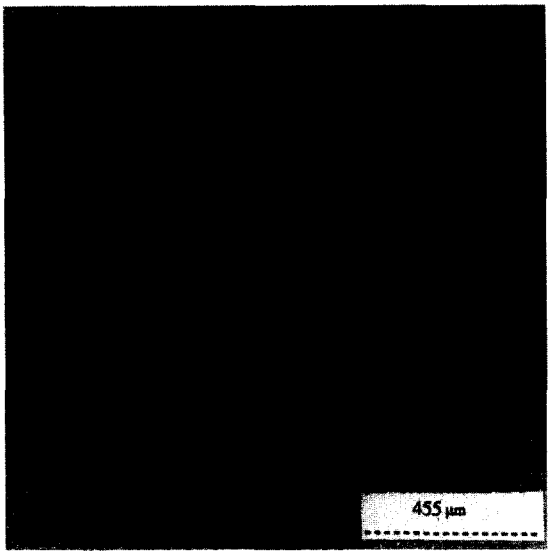

Fig. 26. Theoretical sectional view of porosity of a nickel/alumina catalyst [23].

temperature capillary gas adsorption can be used unchanged.

Whilst several similar 3D networks have been proposed [20–22], the approach in Fig. 25 has been specifically developed to provide images of random slices through such networks. These can then be compared with experimental polished sections viewed on the SEM. In particular, a further three elements of randomness have been incorporated – tortuosity, cross-section shape and surface roughness – so as to provide realistic "virtual reality" sectional images of support porosity like that shown in Fig. 26 for a nickel/alumina reforming catalyst. This recent development has also included a visualisation of porosimetry achieved by low melting point alloy impregnation [23,24] intended to reduce ambiguities typically encountered in interpreting mercury porosimetry. Realistic and visually validated pore networks in 3D should provide a sound basis for analysing the deactivating effects of coke deposition in catalysis.

9. Designing pore-structures to resist deactivation

Issues in catalyst design can be most easily conveyed in two dimensions, although in practise "designed" catalyst pore architecture will be fabricated in 3D. Two brief illustrative examples are given to show the scope for this.

Fig. 27. Pore network designed to resist deactivation [25].

The first illustration in Fig. 27 shows a concept network which, although it is comprised of a full range of pore sizes typical of a stochastic network, has been rearranged into a ranked spiraling assembly with largest pores on the outside and smallest at the centre [25]. Such a porosity structure would accommodate coke deposits accumulating from the outside with a minimum of pore plugging, so that a higher reactivity would be sustained to higher coke levels. The manufacture of such porosity whilst maintaining structural strength is expected to be difficult. Nevertheless, such a potentially more productive particle promises potential gains in reactor performance which are worth pursuing.

The second illustration indicates how a partial amelioration of porous randomness might be achieved by nesting porosity at three levels, as illustrated in Fig. 28. In this example, the largest pore spaces might correspond to monolith dimensions, with two nested stochastic networks forming the porous monolith walls. The interior large network would act like a major highway to provide good transport into the high surface area small pore porosity designed to provide high rates of catalytic reaction. Again, such structural porosity could accommodate coke deposits with good resistance to deactivation.

The detailed specification of optimal geometries for pore structure will require extensions of these simple pore network ideas to include diffusion and surface reaction effects for the formidably complex range of phenomena encountered in industrial reactors. How-

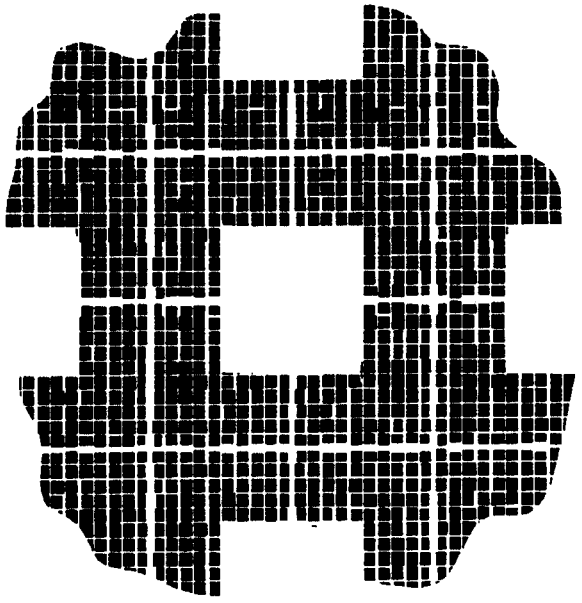

Fig. 28. Three levels of nested porosity [19].

ever, the science and technology of applied catalysis demands that these fundamentals be pursued, if the many ingenious catalytic reactions available to us are to be more effectively exploited.

10. Nomenclature

C	concentration
D	pore diameter
d	coke unit size
D	diffusivity
h	foulant layer thickness (at pore mouth)
i	ith pore (in a network)
k_s	surface reaction rate constant
L	pore length
m	pore connectivity
N_i	net flux (into ith pore)
t_D	time to complete deactivation
x	foulant penetration depth

Greek symbols

β	wedge-layering parameter
λ	average thickness of coke layer
τ_F	dimensionless fouling time
μ	mean pore size

References

[1] A. Voorhies, Carbon formation in catalytic cracking, Ind. Eng. Chem., 37 (1945) 318–322.

[2] O. Levenspiel, Chemical Reaction Engineering, 2nd ed., Wiley, New York, NY, 1972.

[3] G.F. Froment, Catalyst Deactivation, vol. 6, Elsevier, Amsterdam, 1980.

[4] E. Newson, Catalyst deactivation due to pore-plugging by reaction products, Ind. Eng. Chem. Proc. Des. Dev., 14 (1975) 27–33.

[5] F.M. Dautzenberg, J. van Klinken, K.M.A. Pronk, S.T. Sie and J.B. Wijfells, Catalyst deactivation through pore mouth plugging during residue desulfurisation, ACS Symp. Series, 65 (1978) 254–270.

[6] A. Wheeler, Reaction rates and selectivity in catalyst pores, Catalysis, 2 (1955) 105–165.

[7] F.Y.A. El-Kady and R. Mann, Fouling and Deactivation of a FCC Catalyst: A wedge-layering analysis of catalyst particle size LHSV and temperature, Appl. Catal., 3 (1982) 211–234.

[8] C.C. Hughes and R. Mann, Interpretation of Catalyst Deactivation by Fouling from Interactions of Pore Structure and Foulant Deposit Geometries, ACS Symp. Series (Chem. React. Eng., Houston), 65 (1978) 201–213.

[9] V.W. Weekman and D.M. Nace, Kinetics of catalytic cracking selectivity in fixed, moving and fluid bed reactors, Am. Ind. Chem. Eng. J., 16 (1970) 397–404.

[10] D.R. Campbell and B.W. Wojciechowski, Theoretical patterns of selectivity in aging catalysts with special reference to the catalytic cracking of petroleum, Can. J. Chem. Eng., 47 (1969) 413–417.

[11] R. Mann, F.Y.A. El-Kady and R. Marzin, Catalyst deactivation by fouling: A wedge-layering analysis of the consecutive reaction, Chem. Eng. Sci., 40 (1985) 249–257.

[12] R. Mann and G. Thomson, Deactivation of a supported zeolite catalyst: Simulation of diffusion, reaction and coke deposition in a parallel bundle, Chem. Eng. Sci., 42 (1987) 555–563.

[13] J.C.P. Broekhoff and J.H. de Boer, Studies on pore systems in catalysts XI Jl, Catalysis, 10 (1968) 153–165.

[14] G. Thomson, Deactivation of a supported zeolite catalyst: Towards a fundamental approach, Ph.D. Thesis, UMIST (1986).

[15] P.N. Sharratt, Use of network models in the analysis of diffusion, reaction and deactivation in porous catalysts, M.Sc. Thesis UMIST (1985).

[16] R. Mann, G. Thomson and P.N. Sharratt, Deactivation of a supported zeolite catalyst: Diffusion, reaction and coke deposition in stochastic pore networks, Chem. Eng. Sci., 41 (1986) 711–719.

[17] R. Mann, Developments in chemical reaction engineering: Issues related to particle pore structure and porous materials, Trans. Ind. Chem. Eng., 71 (1993) 551–562.

[18] O. Muhammed, Pore structural aspects of catalyst deactivation, PhD. Thesis, UMIST (1993).

[19] R. Mann, Computer-aided characterisation and design of catalyst pore structure, in: A. Cybulski, J.A. Moulijn (Eds.),

Structured Catalysts and Reactors, Marcel Dekker, New York, NY, 1997, Chapter 22, to be published.

[20] M.P. Hollewand and L.F. Gladden, Representation of porous catalysts using random pore networks, Chem. Eng. Sci., 47 (1992) 2757–2762.

[21] S. Arbabi and M. Sahimi, Computer simulation of catalyst deactivation: Effect of morphological, transport and kinetic parameters on the performance of a catalyst, Chem. Eng. Sci., 46 (1991) 1749–1755.

[22] J. Salles, J.E. Thovert and P.M. Adler, Deposition in porous media and clogging, Chem. Eng. Sci., 48 (1993) 2839–2858.

[23] R. Mann, A. Al-Lamy and A. Holt, Visualised porosimetry for pore structure characterisation of a nickel/alumina reforming catalyst, Trans. Ind. Chem. Eng., 73(A) (1995) 147–153.

[24] R. Mann, K. Khalaf and A. Al-Lamy, Evaluation of pore structure geometry and morphology of hydrocarbon conversion catalysts, Intl. Symposium on deactivation and testing of hydrocarbon conversion catalysts, ACS preprints, 40(3) (1995) 516–520.

[25] R. Mann, Fluid catalytic cracking: Some recent developments in catalyst particle design and unit hardware, Catal. Today, 18 (1993) 509–528.